Construction and Building Materials 220 (2019) 565–576

Contents lists available at ScienceDirect

Construction and Building Materials

journal homepage: www.elsevier.com/locate/conbuildmat

Performance of lightweight cement-based and alkali-activated mortars exposed to high-temperature

Chiara Giosuè [a], Alessandra Mobili [a], Costanzo Di Perna [b], Francesca Tittarelli [a,c,*]

[a] Department of Materials, Environmental Sciences and Urban Planning (SIMAU), Università Politecnica delle Marche – INSTM Research Unit, via Brecce Bianche 12, 60121 Ancona, Italy
[b] Department of Industrial Engineering and Mathematical Sciences (DIISM), Università Politecnica delle Marche, via Brecce Bianche 12, 60121 Ancona, Italy
[c] Institute of Atmospheric Sciences and Climate, National Research Council (ISAC-CNR), Via Gobetti 101, 40129 Bologna, Italy

HIGHLIGHTS

- CEM and AAM mortars behave differently at high temperature.
- In CEM mortars, substitution of cement by 40% MK enhances the resistance up to 1000 °C.
- In AAM, substitution of MK by 50% FA enhances the resistance up to 1000 °C.
- The high resistance is due to new crystalline phases formed at high temperatures.

ARTICLE INFO

Article history:
Received 9 April 2019
Received in revised form 27 May 2019
Accepted 31 May 2019
Available online 24 June 2019

Keywords:
Cement
Alkali-activated binders
Lightweight mortars
High temperature behaviour
Fire resistance
Waste valorisation
Mechanical strength
Thermal conductivity
Geopolymer

ABSTRACT

The behavior of lightweight cement-based and alkali-activated mortars after exposure to temperatures of 500, 750, and 1000 °C was compared. In cement-based mortars, cement was partially replaced (40 vol%) by several refractory fillers (coal fly-ash, biomass fly-ash, cocciopesto, metakaolin). In alkali-activated mortars, metakaolin was partially substituted (0, 25, 50 wt%) by coal fly-ash. The substitution of cement by 40% metakaolin and the substitution of metakaolin by 50% fly ash enhances the resistance to high temperatures of cement-based and alkali-activated mortars, respectively. After exposure to 1000 °C, the high residual compressive strength of cement-based mortars with metakaolin is due to the formation of new crystalline species, whereas in alkali-activated mortars is due to their high densification.

1. Introduction

Although cement-based mortars (CEMs) are inorganic materials, their morphological structure, due to crack development or color modification, and chemical composition, considerably change after exposure to very high temperatures, induced, for example, by a fire [1].

In particular, the heating during a fire and the subsequent cooling down after the fire generate thermal gradients, which cause anisotropic thermal expansion that produces microcracking [2]. Furthermore, the rise in temperature causes the following chemical changes:

- at 150 °C: dehydration of calcium silicate hydrate (C-S-H) gel;
- around 450 °C: dehydroxylation of calcium hydroxide (CH);
- at 574 °C: transition in quartz from α to β form;
- around 700 °C: decarbonation of calcium carbonate ($CaCO_3$).

In order to overcome these problems, the use of refractory fillers or aggregates, such as fly ash, silica fume, blast furnace slag [3–5], or lightweight aggregates [6], is suggested. The addition of refractory particles can reduce shrinkage stresses and enhance the mechanical properties of the material after exposure to high temperature [7–9]. The use of lightweight aggregates, such as vermiculite, perlite, pumice, expanded glass, etc., reduces the appar-

* Corresponding author at: Department of Materials, Environmental Sciences and Urban Planning (SIMAU), Università Politecnica delle Marche – INSTM Research Unit, via Brecce Bianche 12, 60121 Ancona, Italy.
E-mail address: f.tittarelli@univpm.it (F. Tittarelli).

https://doi.org/10.1016/j.conbuildmat.2019.05.193
0950-0618/

ent density of composites and consequently the dead loads of structures [10,11], ensuring at the same time higher thermal insulation [12], improved acoustic insulation [13], and higher refractoriness, and, therefore, higher fire resistance. Lightweight aggregates can have natural (pumice or vermiculite) or synthetic origins. Synthetic aggregates can be obtained from natural raw materials (e.g., expanded perlite or expanded clay) or from waste materials (e.g., expanded glass). The use of wastes is recommended to avoid the depletion of natural resources and to increase the sustainability of buildings [14].

The burgeoning attention to environmental impact is leading the construction sector to study durable [15] and alternative binders that are more environmentally friendly [16] compared to ordinary Portland cement [8,17–19]. Alkali-activated materials (AAMs) are clinkerless cement-like compounds obtained by the chemical reaction of a solid aluminosilicate precursor with an alkaline solution generally composed of silicates and sodium or potassium hydroxides [20]. This precursor can be obtained from natural materials, such as metakaolin, or from wastes/by-products, such as blast furnace slag, clay-rich sludges resulting from water treatment or kaolin purification, red mud, coal fly-ash, ground coal bottom-ash, and agricultural waste ashes. Thus, AAMs have lower carbon footprints than CEMs [21].

AAMs have remarkable thermal resistance [22,23], very low thermal conductivity [24], and do not emit toxic fumes when heated [25]. Generally, research on the thermal behavior of AAMs has been mostly focused on AAMs manufactured with metakaolin as a precursor, since metakaolin has a relatively constant chemical composition [26]. However, more recently, AAMs based on fly ash have been attracting interest, since fly ash is a by-product and requires a lower amount of silicate solution than metakaolin to produce AAMs, leading to a further decrease in costs [27].

The thermal behavior of AAMs is affected by multiple variables, including the Si/Al ratio [28], the type of alkali activator [28], and the type of aluminosilicate source used, whether fly ash, metakaolin, or a combination of the two [29].

Although studies have been conducted on the high-temperature behavior of CEMs and AAMs, to the best of the authors' knowledge, studies comparing the thermal resistance of CEMs and AAMs at the same aggregate volume in order to better compare the performances of different binder pastes are missing.

Therefore, this paper compares the effect of exposure to high temperatures on the chemical and mechanical properties of various lightweight mortars prepared with cement or alkali-activated binders, at the same aggregate volume. In particular, CEMs were prepared with a white cement and also partially replaced by several refractory fillers, namely coal fly-ash, biomass fly-ash, cocciopesto, and metakaolin. AAMs were manufactured by the alkali-activation of metakaolin partially substituted with coal fly-ash.

The binder pastes of these mortars were chemically characterized by simultaneous single differential thermal analyses and thermogravimetric analyses (SDTA–TGA) and X-ray diffraction (XRD) before and after exposure to different high temperatures (500, 750, and 1000 °C). The corresponding mortars were characterized in terms of workability, porosity, thermal conductivity, residual compressive strength, modulus of elasticity, and visible changes after the exposure to each temperature.

2. Materials

2.1. Binders

A white cement CEM II B/LL 32.5 R with a density of 3135 kg/m^3 was used as a reference binder (C). Then, alternative binders were prepared by the volumetric substitution of cement with several refractory fillers, namely coal fly-ash (FA-F), biomass fly-ash (FA-B), a cocciopesto filler derived from ceramic fired bricks (CP), and metakaolin (MK).

FA-F (density 2250 kg/m^3, specific surface area 5000 cm^2/g) was provided by a coal-fired power plant located in Northern Italy.

FA-B (density 1410 kg/m^3, specific surface area 3100 cm^2/g) was obtained from an Italian power plant that burns wood for energy production.

CP (density 1270 kg/m^3, specific surface area 28000 cm^2/g) was obtained from red ceramic waste bricks by milling and sieving at 200 μm.

MK (density 2500 kg/m^3, specific surface area 140000 cm^2/g) was MetaStar®501 produced by Imerys Minerals Ltd. (Par, Cornwall, UK), and was obtained by the calcination of kaolinite at 750 °C.

Both FA-F and MK were used as aluminosilicate precursors to prepare alkali-activated pastes and mortars. The alkaline activators were a sodium silicate solution (SS) (molar ratio SiO_2/Na_2O equal to 2.1: SiO_2 = 29.86 wt% and Na_2O = 14.64 wt%) and a potassium hydroxide solution (KOH) of 50 wt% in water.

The chemical compositions of the powdered materials are provided in Table 1.

2.2. Aggregates

The lightweight aggregates were commercially available products manufactured from waste glass, and were produced by Dennert Poraver GmbH (Schlüsselfeld, Germany). The waste glass melting process produces aggregates with encapsulated air pores which provide a high thermal insulating capacity. Three different grain size distributions of expanded glass (EG) were used, labeled as EG A, EG B, and EG C, as reported in Fig. 1.

According to the data sheet, the water absorptions of aggregates required to reach the saturated surface dried condition are: EG A = 35%; EG B = 21%; and EG C = 18% by weight, respectively.

2.3. Mix design

As already suggested by some authors [14,30], lightweight mortars with acceptable mechanical strength can be obtained by using specific mix design tools. One of these studies reported that all the powders, including aggregates and binders, should give a continuous distribution of particles. To obtain the best granulometric size

Table 1
Chemical composition (wt%) of Cement (C) class F Fly Ash (FA-F), biomass Fly Ash (FA-B), Cocciopesto (CP) and Metakaolin (MK).

	SiO_2	Al_2O_3	Fe_2O_3	CaO	MgO	K_2O	Na_2O	TiO_2	SO_3
C	21.9	4.1	0.2	66.0	0.8	0.6	0.3	–	2.3
FA-F	44.2	29.2	7.8	8.5	2.5	1.2	0.4	1.5	1.9
FA-B	17.5	1.7	3.6	46.1	3.7	20.9	<1.0	–	4.7
CP	61.8	16.4	5.5	8.4	2.6	2.3	1.2	0.7	–
MK	55.0	40.2	0.6	<0.1	0.4	2.4	<0.1	–	–

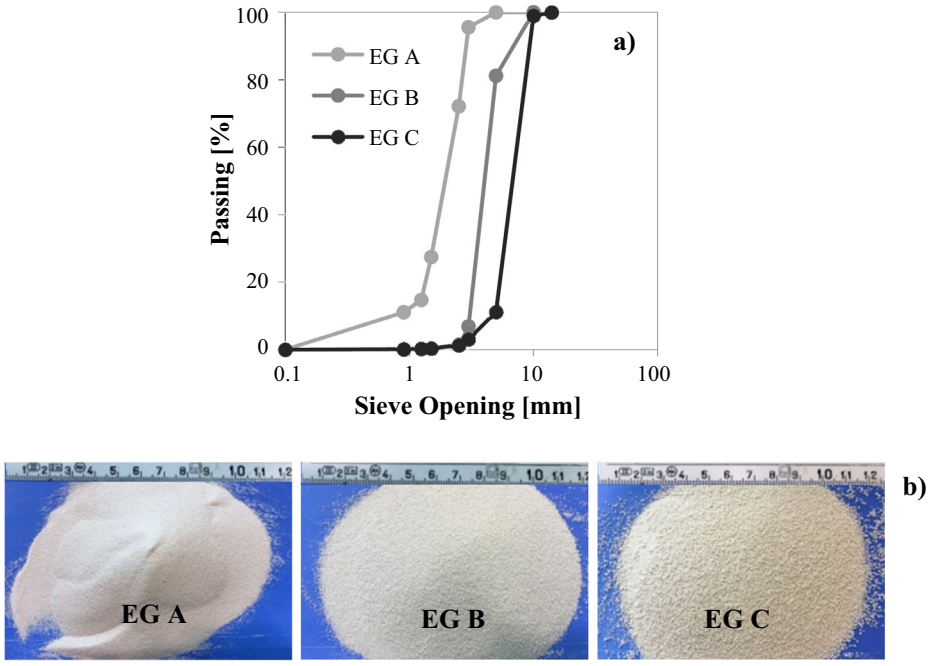

Fig. 1. a) Grain size distributions of the three different fractions and b) corresponding visual aspect.

distribution curve, Funk and Dinger [31] modified the model already developed by Andreasen [32], as:

$$P(D) = \frac{D^q - D^q_{min}}{D^q_{max} - D^q_{min}} \quad (1)$$

where P(D) is the fraction of total solids (binders, powders, and aggregates) for the mixture, D_{min} and D_{max} are the minimum and the maximum diameter (in μm), respectively, suggested by the real granulometric distribution of powders and aggregates, and q is the distribution modulus, which is equal to 0.5, according to previous studies [33].

A cement mortar was used as the reference (100CEM). The volumetric content of the different fractions of solid was evaluated by an optimization algorithm based on the least-squares method (LSM) used by authors in a previous work [33]. Cement was partially replaced by refractory fillers (CP, FA-F, FA-B, and MK) (40% by volume) keeping the same plastic workability (140 ÷ 200 mm) and with a consequent variation of the water/binder (w/b) ratio.

Three alkali-activated mortars were manufactured by substituting MK with FA-F at 0%, 25%, and 50% by weight. The amount of alkaline activator was changed in each mortar in order to maintain the Si/Al and (K + Na)/Al molar ratios at constant values of 1.5 and 1.0, respectively. To compare the alkali-activated mortars with CEMs, the volume of aggregates was kept constant.

The mix proportions of mortars are reported in Table 2.

3. Methods

3.1. Characterization of pastes

3.1.1. Chemical characterization

Pastes were prepared with the same water/powder ratio as was adopted in mortars and were cured in the same way as mortars (see Section 3.2.4).

After curing, to investigate the chemical stability of pastes with increasing temperature, pastes were firstly characterized by SDTA–TGA (STA 409 EP) up to a temperature of 1000 °C with a heating rate of 10 °C/min in an oxidizing environment.

Then, pastes were exposed to temperatures of 500, 750, and 1000 °C in a laboratory electric muffle furnace. The furnace containing specimens was heated by 5 °C/min and held at high temperature for 1 h, and then heating was stopped and the furnace allowed to cool back spontaneously to room temperature. After exposure to high temperature, the crystalline phases of binders can change. The crystalline structures of pastes before and after heating were therefore characterized by XRD analysis using a Rigaku Geigerflex X-ray diffractometer (operating voltage/current 40 kV/30 mA, scan mode continuous speed 3°/min).

Table 2
Mix proportions of mortars (g/L).

Mortars	CEM (g/L)	FA-F (g/L)	FA-B (g/L)	CP (g/L)	MK (g/L)	Activator[a] (g/L)	Water (g/L)	EG[b] (g/L)	w/b[c]
100CEM	539	–	–	–	–	–	256	382	0.47
60CEM 40FA-F	324	156	–	–	–	–	256	382	0.53
60CEM 40FA-B	324	–	98	–	–	–	289	382	0.68
60CEM 40CP	324	–	–	90	–	–	279	382	0.67
60CEM 40MK	324	–	–	–	173	–	378	382	0.76
50MK 50FA-F	–	205	–	–	205	422	–	402	0.40
75MK 25FA-F	–	103	–	–	308	506	–	440	0.50
100MK	–	–	–	–	368	527	–	430	0.58

[a] For alkali-activated mortars the activator is the sum of SS, KOH and mixing water.
[b] The mass of aggregates is in dry condition.
[c] For alkali-activated mortars the binder is the sum of MK, FA-F, and solids dissolved in SS and KOH.

3.2. Characterization of mortars

3.2.1. Workability

The workability of mortars was measured with a truncated conical mold and a jolting table according to the standard UNI EN 1015-3:2007.

3.2.2. Porosity and density

In CEMs, the porosity can be divided into: (a) gel pores-nanopores inside the hydration products, with pore diameters of about 0.5–10 nm; (b) capillary pores-micropores between the hydration products, with pore diameters between 10 nm and 5 μm, strongly dependent on the hydration degree and the w/b ratio; (c) macropores-pores due to entrained air with spherical microbubbles, and (d) pores within the aggregate [34].

The effect of different binders on the pore size distribution of mortars was studied by mercury intrusion porosimetry (MIP) with a PASCAL 240 mercury porosimeter (Thermo Fisher Scientific, Waltham, MA, USA) with a measuring pressure range from 0.01 to 200 MPa. For each mortar type, three small mortar fragments of about 1 cm^3 in volume were tested after 28 days of curing, as described in Section 3.2.4.

After 28 days of curing and after exposure to different temperatures, the density (ρ, in kg/m^3) of hardened mortars was calculated by measuring the dimensions of specimens with a caliper. The volumetric contraction (percentage of volumetric change) was also measured. The reported values are the averages of three measurements.

3.2.3. Thermal transmittance

In order to better characterize mortars at room temperature, their thermal transmittance (λ) was measured according to the standard UNI EN 12664:2002 using cylindrical specimens (d = 130 mm, h = 30 mm) and by evaluating the results with Eq. (2):

$$\lambda = \frac{Jd}{(T_2 - T_1)} \tag{2}$$

where J is the heat flux (W/m^2), d is the distance between thermocouples (m), and T_1 and T_2 are the temperatures at the two different sides of the sample (K).

3.2.4. Mechanical properties

Compressive strength tests were performed according to the standard UNI EN 1015-11:2007 on mortar prisms (40 × 40 × 160 mm) cured at a temperature of 20 ± 2 °C and relative humidity (RH) of 95 ± 5% for seven days, and then at a temperature of 20 ± 2 °C and RH of 65 ± 5% for the following 21 days. A 'Galdabini' hydraulic press with a precision of 1% was used for the compressive strength tests.

Residual mechanical strength was tested after the exposure of mortars to temperatures of 500, 750, and 1000 °C, as described in Section 3.1.1.

In order to evaluate possible damage to specimen structure after exposure to high temperatures, the ultrasonic pulse velocity of specimens was measured [35] to determine the dynamic elastic modulus (E_d) in accordance with the European standard EN 14579:2004. An ultrasonic non-destructive digital indicator tester (PUNDIT) with a measurement resolution of 0.1 μs was used for this purpose. The measurements were conducted in direct mode by putting the two probes on two parallel surfaces of the specimen, to which a thin layer of oil had been previously applied to optimize the contact. Taking into account the obtained ultrasonic pulse velocity (v_s, in m/s), the density of specimens before and after each high-temperature exposure, and the Poisson's modulus γ_d (equal to 0.20 for both cement-based and alkali-activated mortars [16,36]), E_d can be estimated by Eq. (3):

$$E_d = \frac{v_s \rho[(1+\gamma_d)(1-2\gamma_d)]}{(1-\gamma_d)} \tag{3}$$

For the mechanical tests, reported data are the average values of three specimens.

3.2.5. Autoptic analysis

The exposure of specimens to high temperatures can change their macrostructural aspect. The macroscopic aspects of mortar specimens before and after exposure to 500, 750, and 1000 °C were therefore compared by scanning their surfaces with an Epson WF-2630 series scanner.

4. Results and discussion

4.1. Chemical characterization of pastes

Pastes were investigated by SDTA–TGA analysis at temperatures of up to 1000 °C and by XRD analysis after exposure to temperatures of 20, 500, 750, and 1000 °C.

The results of the TGA analysis (Fig. 2) show that all specimens contained different amounts of free water, and evaporating implies a weight loss at around 120 °C [37]. The greatest weight loss was detected in paste 60CEM 40MK (32.2%), followed by all other cement-based pastes: 100CEM (19.5%), 60CEM 40FA-B (19.1%), 60CEM 40FA-F (18.5%), and 60CEM 40CP (18.0%). Alkali-activated pastes showed mass losses of 16.0% for 100MK, 12.0% for 75MK 25FA-F, and 14.0% for 50MK 50FA-F.

A rise in temperature causes strong differences in the behavior of cement-based and alkali-activated binders.

After free-water evaporation, in cement-based pastes, two weight losses were detected, at 420 °C (detected in all pastes except 60CEM 40MK) and at 700 °C, respectively. The weight loss at 420 °C was due to the dehydroxylation of $Ca(OH)_2$. In paste 60CEM 40MK, this weight loss was not detected due to the consumption of portlandite ($Ca(OH)_2$) by reaction with metakaolin [38]. The weight loss at 700 °C was due to the decarbonation of $CaCO_3$ [39]. In the case of 60CEM 40MK, an exothermic peak occurred at around 900 °C without any weight loss (Fig. 2).

In alkali-activated pastes, the weight loss occurred at temperatures below 300 °C. This phenomenon was also observed by Zhang and co-workers [29], who reported that this mass loss is related to the evaporation of chemically bound water. Above 300 °C, no further weight loss was detected in this type of paste. Alkali-activated pastes had lower weight losses than cement-based pastes due to the fact that they were prepared with a lower amount of water, which can evaporate during the curing period.

The results of SDTA analysis (Fig. 2a) for cement-based pastes confirm the results of TGA, with endothermic peaks appearing in correspondence with the respective mass losses (Fig. 2b). In the case of the alkali-activated pastes 50MK 50FA-F, 75MK 25FA-F, and 100MK, a small additional exothermic peak arose at a temperature of 800–900 °C due to the exothermic transformation of amorphous phases into crystalline phases as a consequence of the sintering process [9].

Fig. 3 shows XRD patterns of pastes before and after exposure to elevated temperatures. In the case of cement-based pastes, at room temperature (20 °C), calcite was the most abundant crystalline structure, followed by ettringite ($3CaO{\cdot}Al_2O_3{\cdot}3CaSO_4{\cdot}32H_2O$) and portlandite. The main differences were detected for sample 60CEM 40CP, which is also composed of quartz (SiO_2), and sample 60CEM 40MK, where portlandite is not detected. Concerning alkali-activated pastes, at the same temperature conditions, a

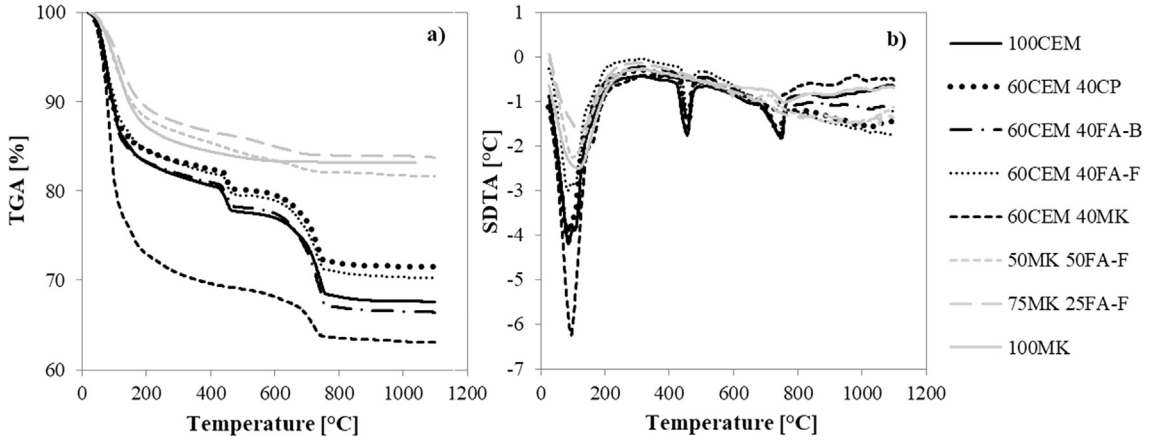

Fig. 2. TGA (a) and SDTA (b) results of pastes.

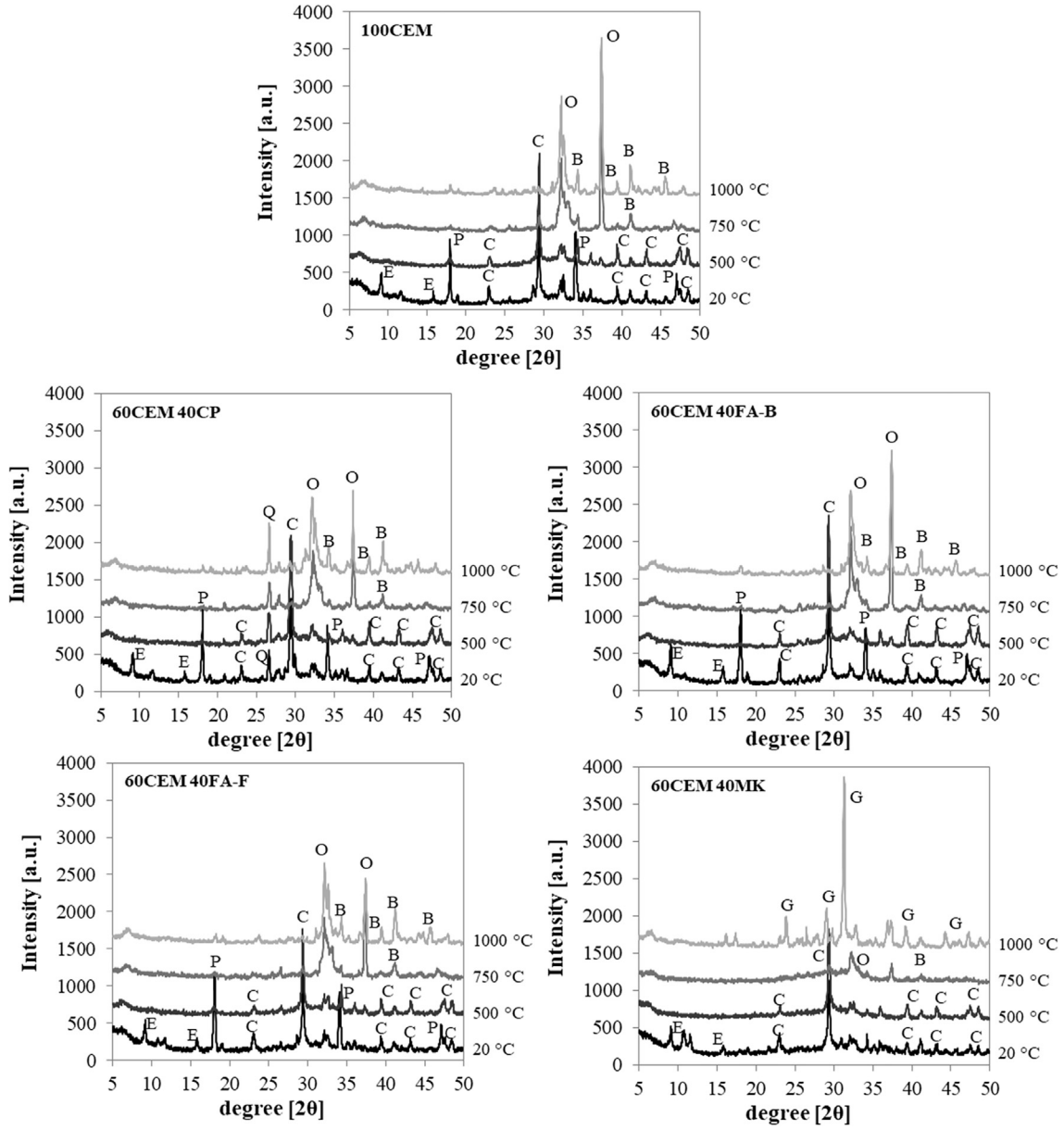

Fig. 3. X-ray diffraction patterns of pastes at 20 °C and after the exposure at different temperature. E: Ettringite, P: Portlandite, C: Calcite, Q: Quartz, O: Calcium Oxide, B: Belite, G: Gehlenite, Ab: Albite, N: Nepheline, L: Leucite.

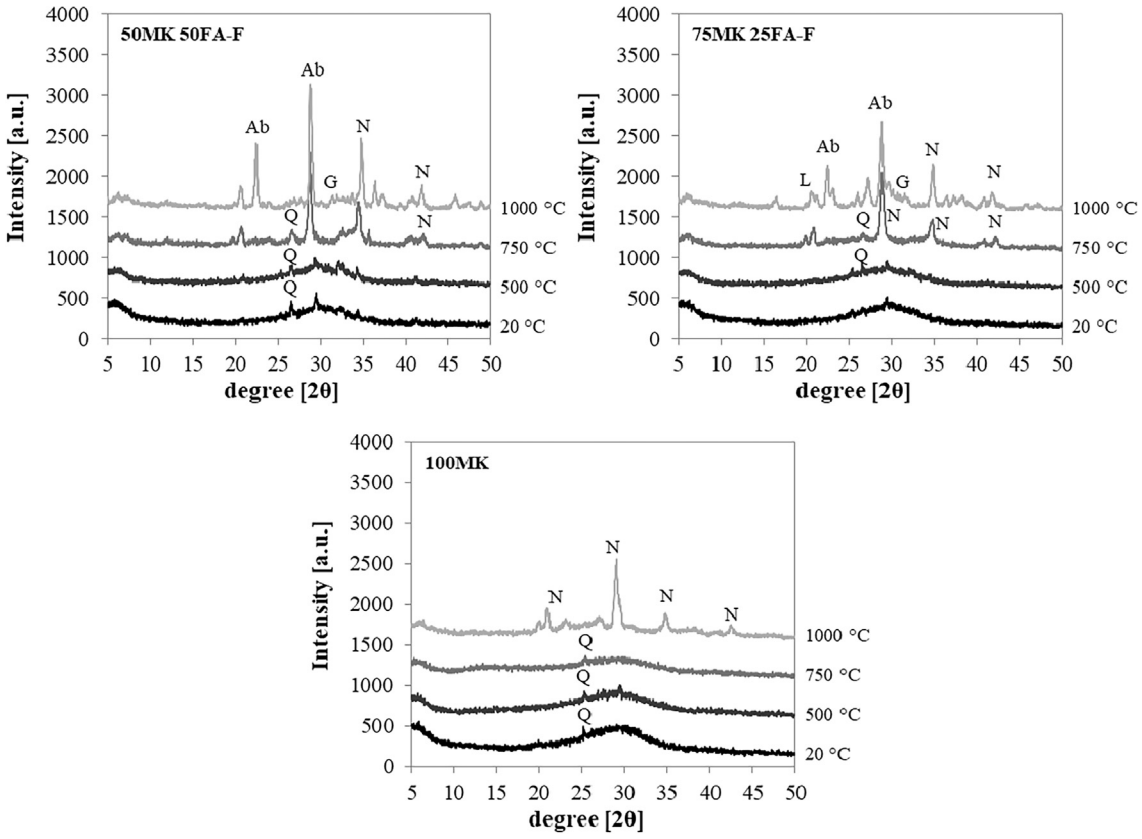

Fig. 3 (*continued*)

marked rise in the XRD pattern baseline suggests the amorphous nature of the binder, which was characterized only by the presence of quartz as a crystalline phase.

After exposure to 500 °C, the XRD patterns of both cement-based and alkali-activated pastes were comparable to those of pastes not exposed to high temperature. In the former, only the disappearance of ettringite occurred, whereas in the latter only a slight reduction in the amount of the amorphous phase was detectable.

Major differences were observed after exposure to temperatures of 750 and 1000 °C. In particular, after exposure to 750 °C, in all cement-based pastes, calcium oxides (CaO) and belite ($2CaO{\cdot}SiO_2$) appeared. Paste 60CEM 40MK showed the lowest amount of CaO, as revealed by the corresponding XRD peaks with the lowest intensity. After exposure to 1000 °C, belite became more visible, and the formation of gehlenite ($Ca_2Al(AlSiO_7)$) was only observed in paste 60CEM 40MK, explaining the exothermic peak detected in SDTA analysis (Fig. 2b). In alkali-activated pastes, the increase of temperature up to 1000 °C caused a substantial change in structure, which transformed from amorphous to crystalline. In paste 100MK, nepheline ($Na_3KAl_4Si_4O_{16}$) was the most abundant crystalline species, whereas when FA-F was added to the paste, albite ($NaAlSi_3O_8$), leucite ($KAlSi_2O_6$), and traces of gehlenite also appeared. The XRD patterns of these specimens confirm the partial crystallization of the alkali-activated phase at elevated temperatures [9], as was also detected in SDTA analysis (Fig. 2b).

4.2. Mortars

4.2.1. Exposure to room temperature (20 °C)

4.2.1.1. Workability. The addition of different amounts of water permits the same workability range to be achieved for different mixes. Slump values fell between 140 and 190 mm (Table 3), which corresponds to the range of plastic consistence (140 ÷ 200 mm) according to the standard UNI EN 1015-6:2007. In particular, the results show that for CEMs, 60CEM 40MK is the least workable, whereas for alkali-activated mortars, 100MK has the lowest slump value. This result is related to the very high specific surface area and fineness of MK, which needs higher quantities of water to wet the surface of MK particles.

4.2.1.2. Porosity and density. The microstructures of mortars were studied at 20 °C in terms of total porosity (Fig. 4a) and cumulative pore size distribution (Fig. 4b).

In general, CEMs had a higher total porosity (V_p) than alkali-activated mortars. Concerning CEMs, in ascending order, 100CEM had a V_p of 53%, followed by 60CEM 40FA-F, with a V_p of 56%, and then by the other mortars, which had V_p values of about 60%. Referring to alkali-activated mortars, 100MK had the highest V_p value (52%), followed by 75MK 25FA-F and 50MK 50FA-F, which had V_p values of 51% and 47%, respectively.

For CEMs, the increased abundance of refractory particles leads to higher porosity. Despite the well-known pozzolanic characteristics of FA-F and MK, higher volumetric additions (40%) lead to higher porosity values [40], explaining also the corresponding lower mechanical strength values.

In alkali-activated mortars, the higher the substitution of MK with FA-F, the lower the total porosity value, since greater amounts of coal fly-ash result in lower water contents being necessary to obtain a certain workability, and consequently lower the amount of free water that can evaporate during the curing process.

The differences between cement-based and alkali-activated mortars are remarkable not only in terms of total porosity, but also pore size distributions. Alkali-activated mortars had smaller pore

Table 3
Workability, hardened density (ρ), thermal transmittance (λ), compressive strength (R_c), and dynamic modulus of elasticity (E_d) of mortars at room temperature.

	Slump (mm)	ρ (kg/m^3)	λ (W/mK)	R_c (MPa)	E_d (MPa)
100CEM	150	1086	0.09	17.2	8536
60CEM 40FA-F	155	1002	0.09	13.1	7460
60CEM 40FA-B	150	852	0.08	8.0	4992
60CEM 40CP	155	859	0.07	8.4	5339
60CEM 40MK	140	1047	0.09	14.4	6844
50MK 50FA-F	185	1268	0.09	22.0	7636
75MK 25FA-F	190	1106	0.08	20.5	6927
100MK	175	1043	0.07	18.4	5279

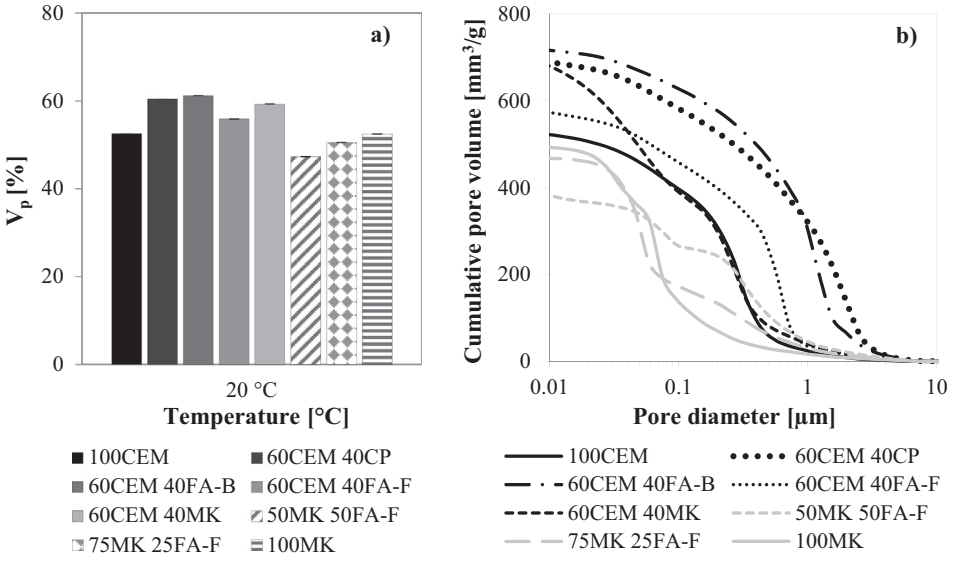

Fig. 4. a) Total volume of accessible pores and b) cumulative pore distribution of mortars at room temperature (20 °C).

diameters than CEMs (their pore distributions were more shifted to the left part of Fig. 4b). In particular, for alkali-activated mortars, increasing the content of MK reduced the number of pores greater than 1 μm in diameter (macropores), probably due to the fact that at room temperature (20 °C) the reactivity of MK is much higher than that of FA-F [41].

The density of the mortars at room temperature (20 °C) is shown in Table 3. In this study, the use of a highly porous aggregate, namely recycled expanded glass, permitted lightweight mortars to be obtained regardless of the binder type [14,30] (ρ < 1300 kg/m^3, according to the standard UNI EN 998-1:2016). CEMs have densities ranging from 800 to 1100 kg/m^3, whereas alkali-activated mortars have densities of around 1000–1300 kg/m^3. The substitution of cement with refractory fillers lowered the density of all CEMs, by about 30% in the case of 60CEM 40CP and 60CEM 40FA-B. The alkali-activated mortar 100MK had a density similar to that of 100CEM, and the density increased with increasing substitution of metakaolin with coal fly-ash. As a matter fact, to obtain a comparable workability of mortars, FA needs less water than MK due to its lower specific surface area; therefore, the resulting w/b ratio decreases (Table 2) giving a less porous (Fig. 5) and denser microstructure.

4.2.1.3. Thermal conductivity. In order to evaluate the thermal conductivity of mortars, the thermal conductivity (λ) was measured at 20 °C. The results are reported in Table 3. Some inorganic insulators are expected to be good materials for fire walls due to their lightness and low thermal properties [42].

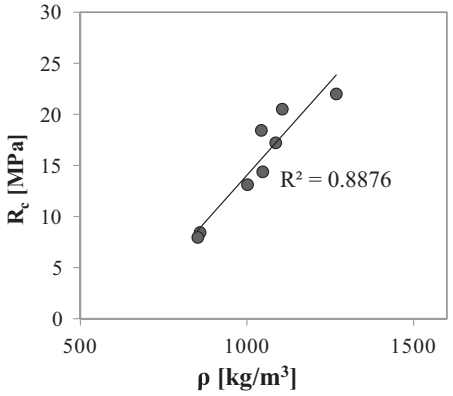

Fig. 5. Correlation between density and compressive strength of mortars at 20 °C.

In the case of CEMs, 100CEM had the highest λ value, 0.09 W/m·K. The other mortar types had similar thermal conductivity values, with the lowest value registered for 100CEM 40CP, 0.07 W/m·K, corresponding to 77% of that of 100CEM. Concerning alkali-activated mortars, 50MK 50FA-F had the highest λ value, 0.09 W/m·K, equal to that of 100CEM, whereas 100MK had the lowest one, equal to that of 60CEM 40CP.

Usually, mortars with a high percentage of voids have strong insulating properties and can be used as plastering joints, building blocks, and panels to guarantee thermal comfort [43]. The correlation between the density and thermal properties of a mortar is well

known: the lower the density, the lower the thermal conductivity [6], since mortars with a lower density contain more air, which has a low thermal conductivity of 0.01 W/m·K [44–47].

In both mortar types (CEMs and alkali-activated mortars), the thermal conductivity is always lower than 0.1 W/m·K, which is the threshold for classifying mortars as T1 thermal insulation mortar according to the standard UNI EN 998-1:2016.

For alkali-activated mortars, increasing the percentage of MK decreased the thermal transmittance due to the lower density of MK (Table 3). The higher water demand of mortars with higher MK content causes a higher free-water content that can evaporate during the curing period, leaving the matrix more porous and hence less dense [16].

4.2.1.4. Mechanical properties. The compressive strength (R_c) of mortars after 28 days of curing at room temperature is reported in Table 3. The results show that 100CEM had a R_c value of 17.2 MPa, whereas the other CEMs had lower R_c values, around 80% (60CEM 40FA-F and 60CEM 40MK) and 50% (60 CEM 40CP and 40CEM 40FA-B) that of 100CEM. At room temperature, alkali-activated mortars exhibited compressive strengths around 10%, 20%, and 30% higher than those of 100MK, 75MK 25FA-F, and 50MK 50FA-F, respectively.

For both cement-based and alkali-activated mortars, compressive strength values followed the w/b ratio (the lower the ratio, the higher the R_c [16]). Moreover, regardless of the type of binder, a linear correlation was found between the compressive strength and density of mortars (Fig. 5). With increasing mechanical strength, the density of mortars increased, owing to the reduced porosity (Table 3). In the case of CEMs, the substitution of cement by refractory fillers lowered the mechanical strength and the density, whereas for alkali-activated mortars, the substitution of metakaolin by fly ash increased both mechanical strength and density.

The results for the dynamic modulus of elasticity (E_d) are reported in Table 3. Mortar 100CEM had the highest E_d value. Mortars 60CEM 40FA-F and 60CEM 40MK had E_d values that were around 10% and 15% lower, respectively, than that of 100CEM, while the other CEMs had values that were about 40% lower. Concerning alkali-activated mortars, 100MK had the lowest E_d value, equal to 60% of that of 100CEM, whereas 75MK 25FA-F and 50MK 50FA-F had E_d values that were 10–20% lower than that of 100CEM (30% and 45% higher, respectively, than that of 100MK).

For CEMs, the addition of refractory fillers decreased the E_d value. The higher the density, the higher the value of R_c and the relative E_d [48]. In alkali-activated mortars, the higher the percentage of FA-F, the higher the E_d value, since the higher amount of fly ash causes an increase in the material's density. According to previous studies, if the R_c values are considered, alkali-activated mortars always have lower E_d values than CEMs with similar mechanical strength [16,19,36,49,50]. As reported by Coppola et al. [51], the reduction of elastic modulus is a consequence of the high shrinkage of alkali-activated mortars which causes microcrack formation.

4.2.2. Exposure to high temperatures (500, 750, and 1000 °C)

4.2.2.1. Density. Fig. 6 shows the density of mortars after exposure to high temperatures.

After exposure to a temperature of 500 °C, all mortars showed a decrease in density, regardless of their composition, whereas after exposure to 750 °C, the densities of most CEMs were unaltered, with the only exception being 60CEM 40MK, whose density increased by about 10%. On the contrary, the densities of alkali-activated mortars slightly increased after exposure to 750 °C.

After exposure to 1000 °C, most CEMs showed a decrease in density, except for 60CEM 40MK, which showed an increase of about 20%. For alkali-activated mortars, those containing FA-F showed a slight increase in density, whereas the one composed entirely of MK showed an increase in density of 50%, and the higher the percentage of MK, the higher the density.

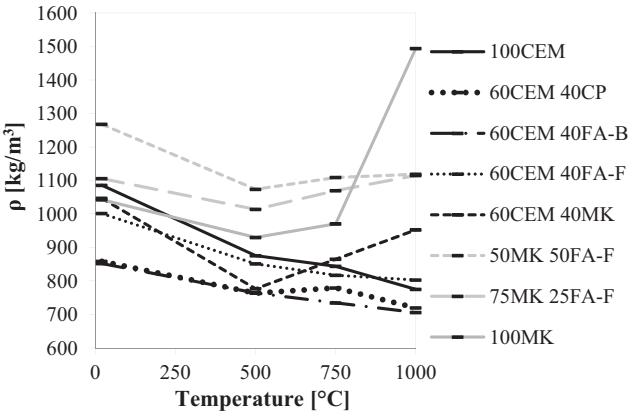

Fig. 6. Density of mortars after the exposure to high temperatures.

For CEMs, increasing the exposure temperature led to a consequent decrease in density, due to the evaporation of non-bound water (mass loss) and the decomposition of the binder, as already discussed in Section 4.1. For alkali-activated mortars, the decrease in density observed after exposure to 500 °C is related to the formation of pores within the matrix [52], whereas the increase in density observed following exposure to higher temperatures, especially when the content of MK was increased, was due to shrinkage. The densification of the matrix was detected not only in alkali-activated mortars but also in 60CEM 40MK.

The volumetric contraction of mortar specimens is shown in Fig. 7. As already reported [53], the structure of cement-based and alkali-activated mortars is stable until exposure to a temperature of 500 °C. After curing at 750 °C, all CEMs showed a contraction of about 5%, except 60CEM 40MK, which showed a contraction of around 20%. For alkali-activated mortars, 50MK 50FA-F showed a general contraction of 10%, and 75MK 25FA-F and 100MK showed contractions of around 20%. The contraction became more evident after exposure to 1000 °C only for mortars containing metakaolin: whereas all mortars seemed to maintain their shape unchanged, 60CEM 40MK and 100MK showed total contractions of 25% and 40% compared to their original volumes, respectively.

In general, the increase in density of alkali-activated mortars and 60CEM 40MK which occurred from 500 to 1000 °C was mainly due to the volume contraction that occurs with the increase in temperature.

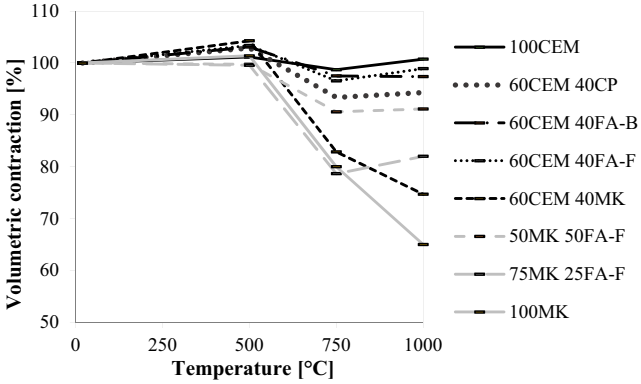

Fig. 7. Volumetric contraction (%) after the exposure to high temperatures.

4.2.2.2. Mechanical properties. After exposure to high temperatures, the residual strength of specimens was tested under compression (Fig. 8a). To allow better analysis of the obtained results, the percentage of residual compressive strength at different temperatures is also reported (Fig. 8b).

In general, for CEMs, a rise in temperature leads to a loss of mechanical performance [53,54]. After exposure to 500 °C, 100CEM experienced a strength reduction of about 15%, similar to that of 60CEM 40FA-F, whereas both 60CEM 40CP and 40CEM 40FA-B showed a R_c value equal to 80% of that at room temperature. Only 60CEM 40MK did not experience a change in compressive strength, probably because it is the only CEM mortar that does not contain portlandite ($Ca(OH)_2$), which decomposes at T = 420 °C, by reaction with metakaolin (Fig. 2a). On the contrary, for alkali-activated mortars, exposure to 500 °C produced a significant drop in compressive strength, with such mortars showing R_c values that were between 65% and 75% lower than those obtained at room temperature, especially for mortars containing higher percentages of MK.

At an exposure temperature of 750 °C, all CEMs except 60CEM 40MK showed a considerable decrease in compressive strength of 20% to 33% compared to their initial strength at 20 °C; 60CEM 40MK maintained a residual R_c of about 60%. Conversely, the residual compressive strength of alkali-activated mortars remained unchanged from 500 to 750 °C.

After exposure to 1000 °C, CEMs experienced a further reduction in compressive strength, reaching values under 3 MPa for the reference mortar 100CEM and for those prepared with FA-F and CP, and lower than 1 MPa for the mortar containing FA-B. Mortar 60CEM 40MK showed the highest compressive strength of all CEMs, around 12 MPa. Alkali-activated mortars showed an opposite trend to CEMs: the compressive strength of 100MK remained unchanged with the rise in temperature, however it became higher with a higher substitution of metakaolin by coal fly-ash. The corresponding R_c values were 8 MPa for 75MK 25FA-F and 13 MPa for 50MK 50FA-F, which are approximately 40% and 60% of their initial values, respectively.

The increase of compressive strength from 750 to 1000 °C of some mixtures is due to the formation of new crystalline phases (Fig. 3) and densification of the matrix (Fig. 6), as explained better in Section 4.2.3.

The variation of mortar E_d with elevated temperature is reported in Fig. 9. After exposure to 500 °C, all mortars showed a decrease in E_d. For CEMs, the decrease in E_d was around 40%, whereas for alkali-activated mortars the decrease was around 70% for 50MK 50FA-F and 80% for both 75MK 25FA-F and 100MK.

After exposure to 750 °C, CEMs maintained their relative E_d trend, and only 60CEM 40MK showed an E_d value higher than that of the reference 100CEM (higher by 40%). The E_d values of alkali-activated mortars were double those after exposure to 500 °C.

After exposure to 1000 °C, CEMs generally had the same E_d values as after exposure to 750 °C, with only that of mortar 60CEM 40MK increasing (doubling compared to the value at room temperature). On the contrary, alkali-activated mortars showed the highest E_d values after exposure to 1000 °C, between five and eight times higher than that of the reference 100CEM.

4.2.2.3. Autoptic evaluation. Images of the surfaces of the mortar specimens after exposure to elevated temperatures are shown in Fig. 10. The formation of cracks was observed in the reference mortar 100CEM after exposure to 1000 °C. The substitution of cement by waste refractory fillers (cocciopesto, biomass and coal fly-ashes) hindered the formation and development of cracks even at the highest temperature, whereas the use of metakaolin was associated with matrix damage at 750 °C. This effect is due to the great volumetric contraction that 60CEM 40MK specimens underwent at both 750 and 1000 °C heating temperatures.

For alkali-activated mortars, cracks were visible especially in 100MK even after exposure to 500 °C. Cracks induced high losses of mechanical performance and developed with the increase of temperature. However, the substitution of metakaolin by coal fly-ash decreased the development of cracks and crack dimension for each exposure temperature.

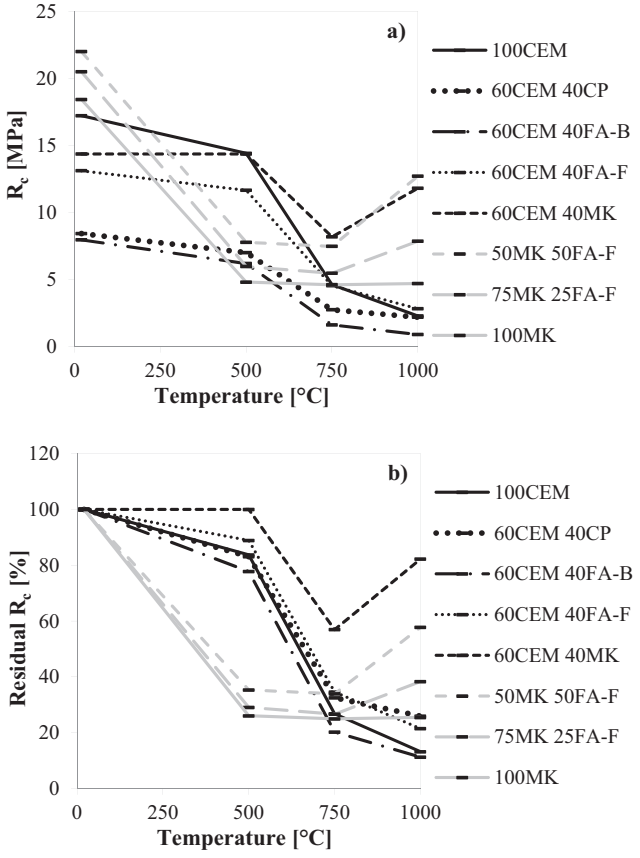

Fig. 8. a) Compressive strength of mortars at room temperature (20 °C) and after the exposure to high temperature and b) percentage of residual compressive strength after the exposure to high temperature.

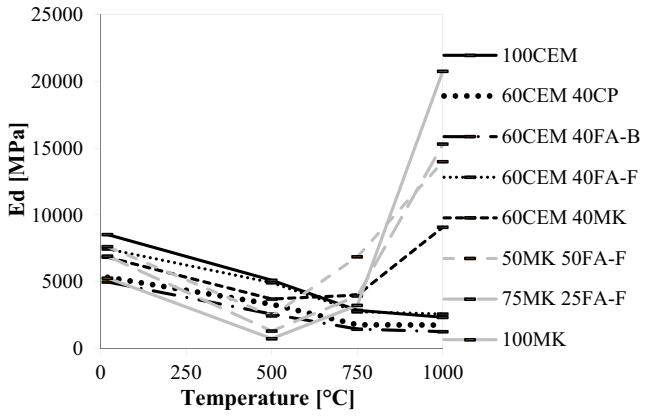

Fig. 9. Dynamic modulus of elasticity (E_d) of mortars at room temperature (20 °C) and after the exposure to high temperature.

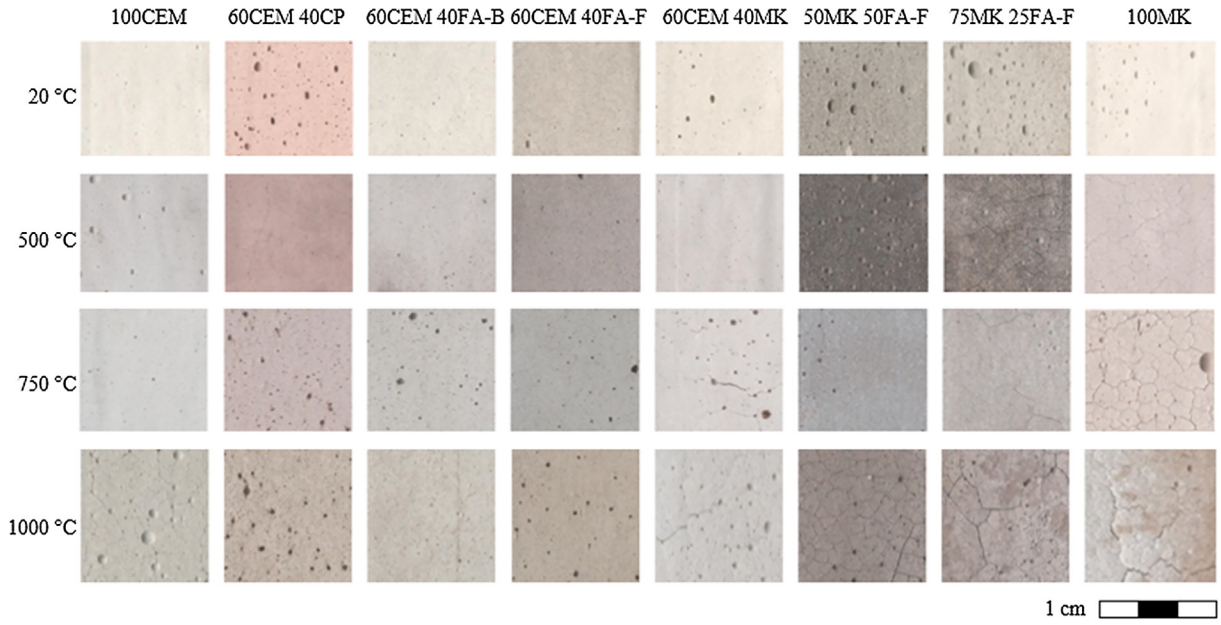

Fig. 10. Visual aspect of mortars acquired by scanning the surface of the specimens after the exposure to the elevated temperatures.

4.2.3. Correlation between mechanical performances and physical and chemical changes in mortars after exposure to high temperatures

When mortars are exposed to high temperatures, the main processes which lead to a reduction in mechanical performance are the chemical decomposition of the binder paste and the development of microcracks [1].

In this work, the decrease in the mechanical performance of CEMs was found to be related to the decomposition of the paste. The loss of compressive strength is caused by the decomposition of calcium silicate hydrates [55]. In CEMs, traces of belite were detected after exposure to 750 °C, and especially after exposure to 1000 °C (Fig. 3). Mortar 60CEM 40MK showed the lowest loss of mechanical performances after each high-temperature exposure, due to the new crystalline phases which formed after the exposure; the appearance of gehlenite was observed in the XRD pattern after exposure to 1000 °C (Fig. 3). Gehlenite is a thermally stable phase which forms after sintering. This process causes material densification, leading to the improvement of mechanical performances [3].

Concerning alkali-activated compounds, the loss of mechanical performance is due to the formation of pores and the presence of diffused cracks within the specimens, which developed after exposure to 500 °C (Fig. 10) [52]. Other authors have reported that metakaolin-based binders often show a decrease in mechanical performances above 200 °C as a consequence of severe shrinkage caused by the dehydration and dehydroxylation of the reaction products. Further exposure to 750 °C induced volume loss (Fig. 7), which was much more pronounced for higher amounts of MK; however, this did not increase the mechanical performance of alkali-activated mortars due to the further development of cracks. After exposure to 1000 °C, alkali-activated mortars showed a high increase in mechanical performances due to the modification of their microstructure. The residual strength of these mortars after exposure to 1000 °C was higher than that measured in CEMs due to the reorganization and subsequent densification of the paste [56], coupled with the formation of new crystalline species such as nepheline, gehlenite, and albite (Fig. 3), which was responsible for the increased compressive strength [57]. Despite the different nature of the binder, when mortar 60CEM 40MK was used, it was possible to obtain a similar performance to that of alkali-activated mortars due to the formation of new crystalline species after exposure to high temperature.

Thermal damage leads to a decrease in E_d in materials with a high content of $Ca(OH)_2$ and $CaCO_3$ [35], which both decompose from 500 °C. This was verified at temperatures up to 1000 °C for all CEMs except 60CEM 40MK. Conversely, alkali-activated mortars showed a different trend: after exposure to 500 °C, the increase in total porosity caused by the development of cracks lowered the dynamic modulus of elasticity. After the exposure to 750 °C, the formation of new crystalline species, as gehlenite in 60CEM 40MK, and the partial crystallization of the amorphous phase in alkali-activated pastes, as detected by XRD patterns (Fig. 3, see Section 4.1), together with shrinkage (Fig. 7) and consequent increase in density (Fig. 6), explain the increase of the E_d of these mixtures after exposure to high temperatures. In general, for both cement-based and alkali-activated mortars, the higher the density, the higher the mechanical resistance.

5. Conclusions

This paper compares the thermal resistances of cement-based and alkali-activated lightweight mortars after exposure to high temperatures (500, 750, and 1000 °C) in terms of chemical composition, porosity, mechanical strength, and visual aspect. Eight different types of mortar were tested: a reference based only on cement, four cement-based mortars prepared by substituting 40% of the cement volume with refractory fillers (metakaolin, cocciopesto, and coal and biomass fly-ashes), and three alkali-activated mortars prepared with metakaolin substituted with 0%, 25%, and 50% of coal fly-ash. In order to obtain lightweight mortars, expanded glass was used as an aggregate.

Briefly, the main conclusions are:

- Cement-based and alkali-activated mortars behaved in different ways when subjected to elevated temperature. For cement-based mortars: The slight reduction of compressive strength after exposure to 500 °C was due to the evaporation of water, and the great strength loss after exposure to 750 °C and 1000 °C was related to the decomposition of the matrix. The substitution of 40% in volume of cement with metakaolin

increased the resistance to high temperature due to the formation of gehlenite, a crystalline phase that is thermally stable at elevated temperatures. For alkali-activated mortars: After exposure to 500 °C, mortars showed a drop in compressive strength due to water evaporation and crack formation; after exposure to 750 °C, the cracks developed, and compressive strength remained the same due to the densification of the matrix; after exposure to 1000 °C, the mechanical performance of the mortars increased due to the change from an amorphous to a crystalline microstructure, with the formation of gehlenite, albite, and nepheline, and the densification of the matrix.

- For CEMs, the partial substitution of cement with cocciopesto and biomass and coal fly-ashes as refractory waste fillers slightly increased the thermal resistance of mortars. Moreover, the use of metakaolin permitted the manufacture of lightweight mortars with a high compressive strength up to temperatures of 1000 °C.
- For alkali-activated mortars, the partial substitution of metakaolin with coal fly-ash increased the thermal resistance up to 1000 °C, lowering the volumetric contraction and the development of cracks and increasing the final compressive strength of specimens compared to those prepared with only metakaolin. The optimal replacement percentage was found to be 50%.
- Despite the use of a different binder, it was possible to obtain similar performances with CEMs and alkali-activated mortars due to the formation of gehlenite, a crystalline phase that is thermally stable at elevated temperatures.

Declaration of Competing Interest

None.

Acknowledgements

The authors wish to thank General Admixture S.p.A. which kindly supplied FA-F, Ingessil S.r.l. which kindly supplied the sodium silicate solution (SS) and Neuvendis S.p.A. which kindly supplied Poraver®.

References

[1] O. Arioz, Effects of elevated temperatures on properties of concrete, Fire Saf. J. 42 (2007) 516–522, https://doi.org/10.1016/j.firesaf.2007.01.003.
[2] W. Yao, H. Liu, Y. Xu, K. Xia, J. Zhu, Thermal degradation of dynamic compressive strength for two mortars, Constr. Build. Mater. 136 (2017) 139–152, https://doi.org/10.1016/j.conbuildmat.2017.01.048.
[3] A. Terzic, L. Pavlovic, Z. Radojevic, V. Pavlovic, V. Mitic, Novel utilization of fly ash for high-temperature mortars: phase composition, microstructure and performances correlation, Int. J. Appl. Ceram. Technol. 12 (2015) 133–146, https://doi.org/10.1111/ijac.12135.
[4] R. Demirboğa, Influence of mineral admixtures on thermal conductivity and compressive strength of mortar, Energy Build. 35 (2003) 189–192, https://doi.org/10.1016/S0378-7788(02)00052-X.
[5] C. García Arenas, M. Marrero, C. Leiva, J. Solís-Guzmán, L.F. Vilches Arenas, High fire resistance in blocks containing coal combustion fly ashes and bottom ash, Waste Manag. 31 (2011) 1783–1789, https://doi.org/10.1016/j.wasman.2011.03.017.
[6] R. Demirboğa, R. Gül, Thermal conductivity and compressive strength of expanded perlite aggregate concrete with mineral admixtures, Energy Build. 35 (2003) 1155–1159, https://doi.org/10.1016/j.enbuild.2003.09.002.
[7] H.E.D.H. Selem, A.M. Rashad, T. Elsokary, Effect of elevated temperature on physico-mechanical properties of blended cement concrete, Constr. Build. Mater. 25 (2011) 1009–1017, https://doi.org/10.1016/j.conbuildmat.2010.06.078.
[8] S.A. Bernal, J. Bejarano, C. Garzón, R. Mejía De Gutiérrez, S. Delvasto, E.D. Rodríguez, Performance of refractory aluminosilicate particle/fiber-reinforced geopolymer composites, Compos. Part B Eng. 43 (2012) 1919–1928, https://doi.org/10.1016/j.compositesb.2012.02.027.
[9] L. Carabba, S. Manzi, E. Rambaldi, G. Ridolfi, M.C. Bignozzi, High-temperature behaviour of alkali-activated composites based on fly ash and recycled refractory particles, J. Ceram. Sci. Technol. 8 (2017) 377–388, https://doi.org/10.4416/JCST2017-00047.
[10] A. Kiliç, C.D. Atiş, E. Yaşar, F. Özcan, High-strength lightweight concrete made with scoria aggregate containing mineral admixtures, Cem. Concr. Res. 33 (2003) 1595–1599, https://doi.org/10.1016/S0008-8846(03)00131-5.
[11] L. Coppola, A. Buoso, D. Coffetti, P. Kara, S. Lorenzi, Electric arc furnace granulated slag for sustainable concrete, Constr. Build. Mater. 123 (2016) 115–119, https://doi.org/10.1016/j.conbuildmat.2016.06.142.
[12] J. Kurnitski, T. Kalamees, J. Palonen, L. Eskola, O. Seppänen, Potential effects of permeable and hygroscopic lightweight structures on thermal comfort and perceived IAQ in a cold climate, Indoor Air 17 (2007) 37–49, https://doi.org/10.1111/j.1600-0668.2006.00447.x.
[13] H.K. Kim, J.H. Jeon, H.K. Lee, Workability, and mechanical, acoustic and thermal properties of lightweight aggregate concrete with a high volume of entrained air, Constr. Build. Mater. 29 (2012) 193–200, https://doi.org/10.1016/j.conbuildmat.2011.08.067.
[14] D.M.A. Huiskes, A. Keulen, Q.L. Yu, H.J.H. Brouwers, Design and performance evaluation of ultra-lightweight geopolymer concrete, Mater. Des. 89 (2016) 516–526, https://doi.org/10.1016/j.matdes.2015.09.167.
[15] F. Tittarelli, A. Mobili, C. Giosuè, A. Belli, T. Bellezze, Corrosion behaviour of bare and galvanized steel in geopolymer and Ordinary Portland Cement based mortars with the same strength class exposed to chlorides, Corros. Sci. 134 (2018) 64–77, https://doi.org/10.1016/j.corsci.2018.02.014.
[16] A. Mobili, A. Belli, C. Giosuè, T. Bellezze, F. Tittarelli, Metakaolin and fly ash alkali-activated mortars compared with cementitious mortars at the same strength class, Cem. Concr. Res. 88 (2016), https://doi.org/10.1016/j.cemconres.2016.07.004.
[17] L. Coppola, T. Bellezze, A. Belli, M.C. Bignozzi, F. Bolzoni, A. Brenna, M. Cabrini, S. Candamano, M. Cappai, D. Caputo, M. Carsana, L. Casnedi, R. Cioffi, O. Cocco, D. Coffetti, F. Colangelo, B. Coppola, V. Corinaldesi, F. Crea, E. Crotti, V. Daniele, S. De Gisi, F. Delogu, M.V. Diamanti, L. Di Maio, R. Di Mundo, L. Di Palma, J. Donnini, I. Farina, C. Ferone, P. Frontera, M. Gastaldi, C. Giosuè, L. Incarnato, B. Liguori, F. Lollini, S. Lorenzi, S. Manzi, O. Marino, M. Marroccoli, M.C. Mascolo, L. Mavilia, A. Mazzoli, F. Medici, P. Meloni, G. Merlonetti, A. Mobili, M. Notarinicola, M. Ormellese, T. Pastore, M.P. Pedeferri, A. Petrella, G. Pia, A. Redeaelli, G. Roviello, P. Scarfato, G. Scoccia, G. Taglieri, A. Telesca, F. Tittarelli, F. Todaro, G. Viliardi, F. Yang, Binders alternative to Portland cement and waste management for sustainable construction – Part 1, J. Appl. Biomater. Funct. Mater. (2018), https://doi.org/10.1177/2280800018782845.
[18] L. Coppola, T. Bellezze, A. Belli, M.C. Bignozzi, F. Bolzoni, A. Brenna, M. Cabrini, S. Candamano, M. Cappai, D. Caputo, M. Carsana, L. Casnedi, R. Cioffi, O. Cocco, D. Coffetti, F. Colangelo, B. Coppola, V. Corinaldesi, F. Crea, E. Crotti, V. Daniele, S. De Gisi, F. Delogu, M.V. Diamanti, L. Di Maio, R. Di Mundo, L. Di Palma, J. Donnini, I. Farina, C. Ferone, P. Frontera, M. Gastaldi, C. Giosuè, L. Incarnato, B. Liguori, F. Lollini, S. Lorenzi, S. Manzi, O. Marino, M. Marroccoli, M.C. Mascolo, L. Mavilia, A. Mazzoli, F. Medici, P. Meloni, G. Merlonetti, A. Mobili, M. Notarinicola, M. Ormellese, T. Pastore, M.P. Pedeferri, A. Petrella, G. Pia, A. Redeaelli, G. Roviello, P. Scarfato, G. Scoccia, G. Taglieri, A. Telesca, F. Tittarelli, F. Todaro, G. Viliardi, F. Yang, Binders alternative to Portland cement and waste management for sustainable construction – Part 2, J. Appl. Biomater. Funct. Mater. (2018), https://doi.org/10.1177/2280800018782852.
[19] A. Mobili, A. Belli, C. Giosuè, A. Telesca, M. Marroccoli, F. Tittarelli, Calcium sulfoaluminate, geopolymeric, and cementitious mortars for structural applications, Environments 4 (2017) 64, https://doi.org/10.3390/environments4030064.
[20] J.L. Provis, Alkali-activated materials, Cem. Concr. Res. 114 (2017) 40–48, https://doi.org/10.1016/j.cemconres.2017.02.009.
[21] B.C. Mclellan, R.P. Williams, J. Lay, A. Van Riessen, G.D. Corder, Costs and carbon emissions for geopolymer pastes in comparison to ordinary portland cement, J. Clean. Prod. 19 (2011) 1080–1090, https://doi.org/10.1016/j.jclepro.2011.02.010.
[22] X. Yao, Z. Zhang, H. Zhu, Y. Chen, Geopolymerization process of alkali – metakaolinite characterized by isothermal calorimetry, Thermochim. Acta 493 (2009) 49–54, https://doi.org/10.1016/j.tca.2009.04.002.
[23] A. Natali Murri, W.D.A. Rickard, M.C. Bignozzi, A. van Riessen, High temperature behaviour of ambient cured alkali-activated materials based on ladle slag, Cem. Concr. Res. 43 (2013) 51–61.
[24] P. Duxson, A. Fernández-Jiménez, J.L. Provis, G.C. Lukey, A. Palomo, J.S.J. van Deventer, Geopolymer technology: the current state of the art, J. Mater. Sci. 42 (2007) 2917–2933, https://doi.org/10.1007/s10853-006-0637-z.
[25] P. Duxson, J.L. Provis, G.C. Lukey, J.S.J. Van Deventer, The role of inorganic polymer technology in the development of 'green concrete', Cem. Concr. Res. 37 (2007) 1590–1597, https://doi.org/10.1016/j.cemconres.2007.08.018.
[26] C. Kuenzel, L. Li, L. Vandeperre, A.R. Boccaccini, C.R. Cheeseman, Influence of sand on the mechanical properties of metakaolin geopolymers, Constr. Build. Mater. 66 (2014) 442–446, https://doi.org/10.1016/j.conbuildmat.2014.05.058.
[27] G. Habert, J.B. d'Espinose de Lacaillerie, N. Roussel, An environmental evaluation of geopolymer based concrete production: reviewing current research trends, J. Clean. Prod. 19 (2011) 1229–1238, https://doi.org/10.1016/j.jclepro.2011.03.012.
[28] D.L.Y. Kong, J.G. Sanjayan, K. Sagoe-Crentsil, Factors affecting the performance of metakaolin geopolymers exposed to elevated temperatures, J. Mater. Sci. 43 (2008) 824–831, https://doi.org/10.1007/s10853-007-2205-6.
[29] H.Y. Zhang, V. Kodur, S.L. Qi, L. Cao, B. Wu, Development of metakaolin-fly ash based geopolymers for fire resistance applications, Constr. Build. Mater. 55 (2014) 38–45, https://doi.org/10.1016/j.conbuildmat.2014.01.040.

[30] Q.L. Yu, P. Spiesz, H.J.H. Brouwers, Ultra-lightweight concrete: conceptual design and performance evaluation, Cem. Concr. Compos. 61 (2015) 18–28, https://doi.org/10.1016/j.cemconcomp.2015.04.012.
[31] J.E. Funk, D.R. Dinger, Predictive Process Control of Crowded Particulate Suspensions: Applied to Ceramic Manufacturing, Kluwer Academic, USA, 1994.
[32] A.H.M. Andreasen, Ueber die Beziehung zwischen Kornabstufung und Zwischenraum in Produkten aus losen Kornern (mit einigen Experimenten), Kolloid-Zeitschrift 50 (1930) 217–228, https://doi.org/10.1007/BF01422986.
[33] C. Giosuè, Q.L. Yu, M.L. Ruello, F. Tittarelli, H.J.H. Brouwers, Effect of pore structure on the performance of photocatalytic lightweight lime-based finishing mortar, Constr. Build. Mater. 171 (2018) 232–242, https://doi.org/10.1016/j.conbuildmat.2018.03.106.
[34] R. Kumar, B. Bhattacharjee, Porosity, pore size distribution and in-situ strength of concrete, Cem. Concr. Res. 33 (2003) 155–164, https://doi.org/10.1016/S0008-8846(02)00942-0.
[35] A. Bonazza, G. Vidorni, I. Natali, C. Ciantelli, C. Giosuè, F. Tittarelli, Durability assessment to environmental impact of nano-structured consolidants on Carrara marble by field exposure tests, Sci. Total Environ. 575 (2017) 23–32, https://doi.org/10.1016/j.scitotenv.2016.10.004.
[36] A. Mobili, C. Giosuè, M. Bitetti, F. Tittarelli, Cement mortars and geopolymers with the same strength class, Proc. Inst. Civ. Eng. Constr. Mater. 169 (2016), https://doi.org/10.1680/coma.14.00063.
[37] L. Alarcon-Ruiz, G. Platret, E. Massieu, A. Ehrlacher, The use of thermal analysis in assessing the effect of temperature on a cement paste, Cem. Concr. Res. 35 (2005) 609–613, https://doi.org/10.1016/j.cemconres.2004.06.015.
[38] S. Wild, J.M. Khatib, Portlandite consumption in metakaolin cement pastes and mortars, Cem. Concr. Res. 27 (1997) 137–146.
[39] M. Arandigoyen, J.L. Pérez Bernal, M.A. Bello Lopez, J.I. Alvarez, Lime-pastes with different kneading water: pore structure and capillary porosity, Appl. Surf. Sci. 252 (2005) 1449–1459, https://doi.org/10.1016/j.apsusc.2005.02.145.
[40] P. Chindaprasirt, S. Rukzon, Strength, porosity and corrosion resistance of ternary blend Portland cement, rice husk ash and fly ash mortar, Constr. Build. Mater. 22 (2008) 1601–1606, https://doi.org/10.1016/j.conbuildmat.2007.06.010.
[41] R.R. Lloyd, Accelerated ageing of geopolymers, in: L. Provis, J.S.J. van Deventer (Eds.), Geopolymers Struct. Process. Prop. Ind. Appl., Elsevier, 2009, pp. 139–166, https://doi.org/10.1533/9781845696382.2.139.
[42] C. Ferna, C. Leiva, L.F. Vilches, Fire resistance of biomass ash panels used for internal partitions in buildings, Fire Saf. J. 44 (2009) 622–628, https://doi.org/10.1016/j.firesaf.2008.12.005.
[43] S. Aydin, B. Baradan, Effect of pumice and fly ash incorporation on high temperature resistance of cement based mortars, Cem. Concr. Res. 37 (2007) 988–995, https://doi.org/10.1016/j.cemconres.2007.02.005.
[44] W.D.A. Rickard, L. Vickers, A. Van Riessen, Performance of fibre reinforced, low density metakaolin geopolymers under simulated fire conditions, Appl. Clay Sci. 73 (2013) 71–77, https://doi.org/10.1016/j.clay.2012.10.006.
[45] M.F. Ashby, H. Shercliff, D. Cebon, Agitated atoms: materials and heat, in: Mater. Eng. Sci. Process. Des., third ed., Butterworth-Heinemann, Oxford, 2009, p. 257.
[46] F. Tittarelli, Effect of low dosages of waste GRP dust on fresh and hardened properties of mortars: Part 2, Constr. Build. Mater. 47 (2013) 1539–1543, https://doi.org/10.1016/j.conbuildmat.2013.06.086.
[47] F. Tittarelli, C. Giosuè, A. Mobili, C. di Perna, S. Monosi, Effect of using recycled instead of virgin EPS in lightweight mortars, Procedia Eng. 161 (2016) 660–665, https://doi.org/10.1016/j.proeng.2016.08.728.
[48] F. Demir, A new way of prediction elastic modulus of normal and high strength concrete-fuzzy logic, Cem. Concr. Res. 35 (2005) 1531–1538, https://doi.org/10.1016/j.cemconres.2005.01.001.
[49] A. Mobili, C. Giosuè, A. Belli, T. Bellezze, F. Tittarelli, Geopolymeric and cementitious mortars with the same mechanical strength class: performances and corrosion behaviour of black and galvanized steel bars, Am. Concr. Institute, ACI Spec. Publ., 2015.
[50] P. Nath, P.K. Sarker, Flexural strength and elastic modulus of ambient-cured blended low-calcium fly ash geopolymer concrete, Constr. Build. Mater. 130 (2017) 22–31, https://doi.org/10.1016/j.conbuildmat.2016.11.034.
[51] L. Coppola, D. Coffetti, E. Crotti, Pre-packed alkali activated cement-free mortars for repair of existing masonry buildings and concrete structures, Constr. Build. Mater. 173 (2018) 111–117, https://doi.org/10.1016/j.conbuildmat.2018.04.034.
[52] Y. Luna-Galiano, A. Cornejo, C. Leiva, L.F. Vilches Arenas, C. Fernández Pereira, Properties of fly ash and metakaolín based geopolymer panels under fire resistance tests, Mater. Constr. 65 (2015) 3, https://doi.org/10.3989/mc.2015.06114.
[53] B. Jeyaprabha, G. Elangovan, P. Prakash, Strength and microstructure of fired mortars with river sand alternatives after air cooling, Mater. Struct. 50 (2017) 76, https://doi.org/10.1617/s11527-016-0886-5.
[54] A. Lotfy, K.M.A. Hossain, M. Lachemi, Durability properties of lightweight self-consolidating concrete developed with three types of aggregates, Constr. Build. Mater. 106 (2016) 43–54, https://doi.org/10.1016/j.conbuildmat.2015.12.118.
[55] G.F. Peng, Z.S. Huang, Change in microstructure of hardened cement paste subjected to elevated temperatures, Constr. Build. Mater. 22 (2008) 593–599, https://doi.org/10.1016/j.conbuildmat.2006.11.002.
[56] P. Duxson, G.C. Lukey, J.S.J. Van Deventer, Physical evolution of Na-geopolymer derived from metakaolin up to 1000 °C, J. Mater. Sci. 42 (2007) 3044–3054, https://doi.org/10.1007/s10853-006-0535-4.
[57] A. Fernández-Jiménez, J.Y. Pastor, A. Martín, A. Palomo, High-temperature resistance in alkali-activated cement, J. Am. Ceram. Soc. 93 (2010) 3411–3417, https://doi.org/10.1111/j.1551-2916.2010.03887.x.